

A Low Complexity Full-Duplex Radio Implementation with a Single Antenna

Muhammad Sohaib, Haq Nawaz, Kerem Ozsoy, Ozgur Gurbuz *Member, IEEE*, Ibrahim Tekin, *Member, IEEE*

Abstract—This work presents a novel low complexity full-duplex radio design, which only uses a single patch antenna without any duplexer or circulator for passive suppression of self-interference, and a computationally efficient technique for linear digital cancellation. The proposed full-duplex design is tested for IEEE 802.11g wireless standard, on the WARP (v3) software defined radio implementation platform. It is shown that this design provides a total suppression of 88 dB, which is sufficient for low power or short range full-duplex communication. The dual polarized slot coupled patch antenna used in our design provides an inter-port isolation as high as 60 dB in 2.4 GHz band. Additionally, the digital domain cancellation utilizes a frequency domain based estimation and reconstruction approach, which not only offers up to 61% reduction in the computational complexity but also provide a 5–7 dB better digital cancellation performance in highly selective channel conditions, as compared to the time domain based techniques. The proposed full-duplex implementation can be easily applied in OFDM based wireless systems, such as IEEE 802.11, which is the considered air interface in this work.

Index Terms—Full-Duplex, Self-Interference, Passive Suppression, Digital Domain Cancellation, Fading Channels.

I. INTRODUCTION

A. Motivation and Contributions

In recent years, significant number of wireless network users have replaced their phones with the trending smart phones and similar devices, which has resulted in the dramatic increase in wireless data traffic. As the current systems strive to fulfill this growing demand, researchers in both industry and academia are investigating new technologies for providing higher capacity, and full-duplex communication is one of the emerging technologies with the potential to arbitrate the present wireless spectral congestion. A full-duplex radio, which transmits and receives simultaneously over the same frequency band, ideally cuts the spectrum requirement to half, i.e., it can either double the spectral efficiency of a half-duplex system, or it has the capacity to accommodate twice the number of users in the same cell zone.

Until recently, the very idea of full-duplex wireless transmission was considered impossible. For this reason, all radios were designed to operate in half-duplex mode, which requires

separate resources in time or frequency for reliable transmission and reception. The major problem that has impeded the implementation of full-duplex is the self-interference signal generated by a radio's own transmission, received at a power level much higher than that of the desired received signal arriving from a distant transmitting antenna. Since the self-interference signal travels much shorter distance, it can be over a million times stronger than the desired signal, and more or less occupies the whole dynamic range of the analog-to-digital converters (ADC) in the received signal processing path, making the processing of the desired signal impossible. To enable full-duplex communication, a radio is required to suppress the self-interference signal to the receiver's noise floor. Any residual self-interference raises the noise floor for the desired signal, which results in reduced signal-to-noise ratio (SNR), and lower system throughput.

In this article, we present a novel low complexity single antenna full-duplex radio design, where passive suppression is employed with a patch antenna, and active digital cancellation is achieved with frequency domain based estimation and reconstruction of the self-interference signal. The contributions of this work can be summarized as follows:

- For passive suppression, a single antenna is employed without a circulator/duplexer element and complex active analog cancellation hardware. Our solution with the dual polarized slot coupled antenna can provide an isolation of 56–60 dB in IEEE 802.11g 2.4 GHz wireless band.
- For linear digital cancellation, frequency domain estimation is implemented and a frequency domain reconstruction technique is proposed, which not only offers reduced complexity cost that is one third of the complexity of the existing techniques, but it outperforms the existing techniques by providing 5–7 dB higher digital cancellation in frequency selective fading channels.
- Proposed passive suppression and digital cancellation techniques are implemented and integrated on a WARP (v3) radio board and the self-interference suppression performance of the full-duplex implementation is evaluated, considering different digital cancellation algorithms and different practical transmit power settings.
- Our test results show that the proposed full-duplex radio design can achieve a total self-interference cancellation up to 88 dB, which is sufficient for enabling full-duplex communication for medium to low power levels.
- The proposed design can easily enable full-duplex for any orthogonal frequency division multiplexing (OFDM) based wireless system at low cost, since it only requires

Copyright (c) 2015 IEEE. Personal use of this material is permitted. However, permission to use this material for any other purposes must be obtained from the IEEE by sending a request to pubs-permissions@ieee.org.

This work was supported in parts by TUBITAK Grant No 215E326 and TUBITAK BIDEB 2215.

Muhammad Sohaib, Haq Nawaz, Ozgur Gurbuz, Ibrahim Tekin are with Faculty of Engineering and Natural Sciences, Sabanci University, Istanbul, Turkey (e-mail: muhammadsahaib, hnawaz, ogurbuz, tekin@sabanciuniv.edu).

Kerem Ozsoy is with Antsis Electronics, Istanbul Turkey (e-mail: kerem.ozsoy@antsiselektronik.com.tr).

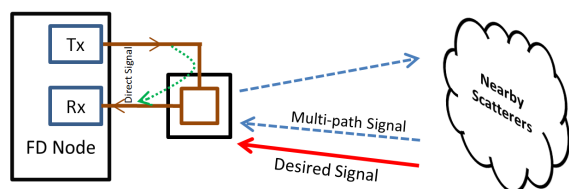


Fig. 1: Received signals at the receiver of a full-duplex node.

minimal changes in the digital baseband hardware and just a single antenna, with no additional analog circuitry.

B. Background and Related Work

At the receiver of a full-duplex radio, the received signal can be decomposed into three components [1]: the desired signal, the direct self-interfering signal due to limited RF isolation and the reflected (multi-path) self-interfering signals, as illustrated in Fig 1. The self-interference signals observed at the receiver are nothing but the distorted versions of the (known) transmitted signal, and these distortions which can be both linear and nonlinear, are mainly caused by the transmit chain and the channel. Recent works [2]–[13] have presented different techniques and system architectures to suppress this self-interference for reliable full-duplex transmission. The self-interference suppression techniques can be categorized as passive suppression and active cancellation.

In passive suppression, self-interference is suppressed in the propagation domain, at the radio frequency (RF) level [2]. A passive suppression technique can mitigate the direct/leaked self-interference signal to a great extent; however, it cannot repress the reflected self-interference component. For passive suppression, prior designs have either used two antennas [7]–[13], or a single antenna connected via circulator/duplexer [3]–[7]. The former designs provide self-interference suppression either by the electromagnetic isolation of the transmitted and received signals through antenna separation (with/without RF absorbers) along with antenna position and directivity adjustment (73 dB of RF isolation [10]) or by using balanced/unbalanced (Balun) transformer providing 45 dB suppression in 40 MHz bandwidth [12]. However, using more than one antenna for full-duplex communication weakens its purpose, since two or more antennas can themselves be used to double the throughput using MIMO structures in half-duplex mode. The latter circulator/duplexer based single antenna designs are not only expensive but they provide limited passive suppression (10 – 15 dB as given in [5]–[7], and 36 dB in [4]), hence additional analog cancellation circuitry becomes a definite requirement to obtain the desired levels of suppression.

The active cancellation technique, on the other hand, eliminates self-interference by subtracting a processed copy of the transmitted signal from the received signal. Active cancellation is further divided into two stages: analog domain cancellation and digital domain cancellation. Analog domain cancellation is achieved in [3], [6], [12] with an analog cancellation circuit, which taps the transmit chain (after the power amplifier) to obtain a small copy of the transmitted signal just before the antenna, thus capturing the transmit chain impairments,

such as power amplifier nonlinearities. The full-duplex designs proposed in [11] and [13] use an auxiliary transmit chain for modeling the self-interference signal, which also alleviate phase noise effect due to common oscillator. Both approaches of analog cancellation offer improved overall cancellation; however, they not only require calibration (increasing the design complexity), but bring additional hardware with active elements as well. Due to additional circuitry for such analog cancellation, the complexity, cost, size and power consumption of the overall design are to be increased. The passive suppression stage of our full duplex design is much simpler than the above mentioned works, since RF level suppression is obtained without using duplexer/circulator or any additional circuitry.

For digital cancellation in full-duplex radios, a discrete time system is modeled using transmitted preamble, which captures the effects of all stages from the digital-to-analog converter (DAC) at the transmitter side until the ADC at the receiver side, as well as the multi-path channel in between. Using this discrete system and the known transmitted samples an approximate self-interference signal is first reconstructed, and then it is subtracted from the received baseband samples. In most of the previous works as well as in our design, modeling of the linear self-interference component is considered only. However, in [3], [6], [8], nonlinear self-interference component is also modeled, and improved overall cancellation performance is demonstrated. Nevertheless, this improvement comes at the cost of significantly increased complexity, since the computational requirements for nonlinear self-interference cancellation grows exponentially with nonlinear order, as shown at the end of Section III. With the goal of achieving full-duplex communication at lowest complexity, only linear digital cancellation is considered in this work. In [14], a frequency domain based self-interference reconstruction approach for linear cancellation is proposed, and compared in terms of performance and complexity with the digital cancellation techniques employed in [5], [6], [12].

This article extends the performance analysis done in [14] by including comparisons of digital cancellation performance using other self-interference channel estimation schemes from the literature, and by considering the effect of training symbol length on estimation performance for all algorithms. Furthermore, all the evaluated digital cancellation algorithms are implemented on the WARP radio board in integration with passive suppression, the dual port, dual polarized slot coupled antenna, resulting in a single antenna full duplex radio. The cancellation performance of the proposed full-duplex system is evaluated on the WARP setup with over the air tests and tests with a channel emulator incorporating the IEEE 802.11 indoor channel model effects.

C. Paper Organization

The rest of the paper is organized as follows: Section II provides the details of our dual polarized slot coupled patch antenna. Section III covers the different techniques for linear digital cancellation, their performance via simulations and complexity analysis. In Section IV, the single antenna full

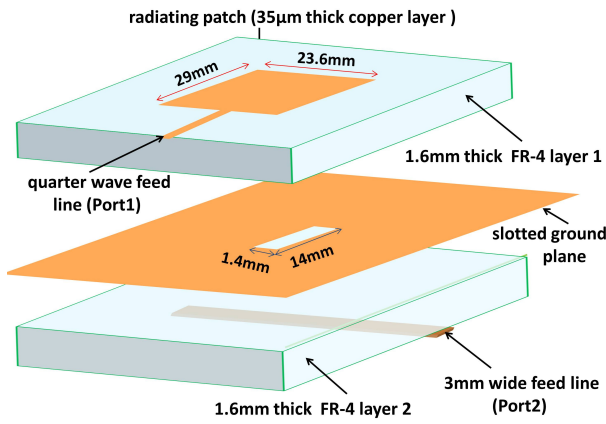


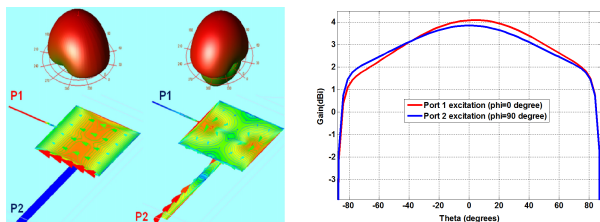
Fig. 2: Geometry of dual port patch antenna with one microstrip fed port and one slot coupled port.

duplex radio design, with implementation and integration of proposed passive suppression and digital cancellation, is presented. The test results obtained with our design are presented in Section V, and conclusions are provided in Section VI.

II. PASSIVE SUPPRESSION OF SELF-INTERFERENCE

For passive suppression of the self-interference signal, we have designed a dual polarized slot coupled patch antenna, which has the capacity to provide significant self-interference suppression (up-to 60 dB) in the IEEE 802.11g standard operational frequency band. Our dual polarized patch antenna uses one thin quarter-wave microstrip feed for one polarization while the aperture coupled configuration which excites the antenna through a small slot in the ground plane is used for second polarization. The dual polarized patch antenna with such hybrid feeding mechanism provides improved inter-port isolation as compared to patch antenna with two perpendicular thin quarter-wave microstrip feeds [15]. For aperture coupled port, the shape and size of aperture in ground plane defines the amount of coupling from feed to radiating patch [16], [17].

The structure of our proposed dual polarized patch antenna with optimized dimensions is shown in Fig. 2, which consists of two 1.6mm thick FR-4 substrate ($\epsilon = 4.4$, tangent loss = .02) layers. The design is simulated using Keysight Advanced Design System (ADS) Momentum software. The simulated



(a) 3-D gain pattern of each port.(b) 2-D gain patterns at 2.4 GHz.

Fig. 3: Simulated surface currents, 3-D gain patterns and 2-D gain patterns of the dual polarized slot coupled microstrip antenna at 2.4 GHz frequency.

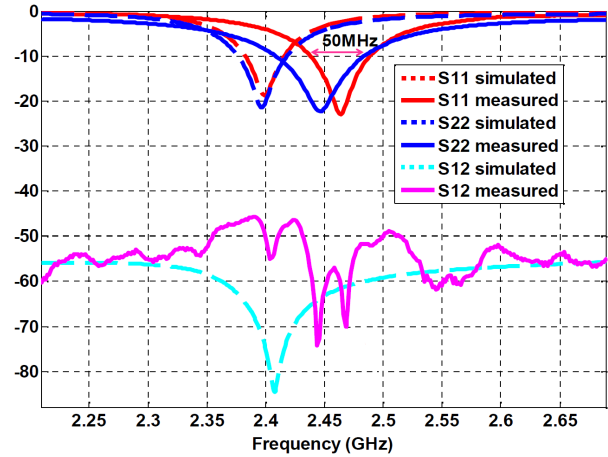


Fig. 4: Simulated and measured S_{11} , S_{22} and S_{12} parameters for dual polarized slot coupled microstrip antenna.

surface currents, 3-D gain patterns and 2-D gain patterns of the dual polarized microstrip antenna for each port excitation while the other port terminated with 50 ohms are shown in Fig. 3. The proposed antenna provides 4.1 dB and 3.8 dB gain for microstrip fed port and slot coupled port at 2.4 GHz frequency for each polarization ($\Phi = 0^\circ$ and $\Phi = 90^\circ$) respectively.

The simulated and measured S-parameter (S_{11} , S_{22} and S_{12}) results for the proposed and implemented dual polarized slot coupled antenna are shown in Fig. 4. The quarter wave microstrip fed (port 1) and slot coupled port (port 2) have 50 MHz and 100 MHz input 10 dB impedance-bandwidths respectively. The fabricated antenna provides around 70 dB inter-port isolation at center frequency and port to port is more than 55 dB for antenna's 10 dB impedance bandwidth of 50 MHz. There is a nice agreement between simulated and measured results except the measured and simulated inter-port isolation results, which differ because the implemented antenna has finite slotted ground plane while the simulation results were obtained with infinite ground plane.

III. DIGITAL SELF-INTERFERENCE CANCELLATION

The digital self-interference cancellation plays a concluding role in full-duplex implementation as it primarily quantifies the SNR, and henceforth the throughput of the system. The regeneration of self-interference in digital domain is a two step process, first the self-interference channel is estimated using the long training sequence (LTS) symbols, embedded in the preamble of the transmitted OFDM packet. Afterwards, the acquired estimate is processed with the known transmitted samples/symbols to reconstruct an approximate self-interfering signal on the receiving side. The quality of the reconstructed signal, in terms of proximity with the actual self-interfering signal, essentially depends on the accuracy of the estimate, thus making channel estimation process a crucial stage for obtaining substantial digital self-interference cancellation. We present the baseband system model of our full-duplex radio first, providing signal/packet structures, building blocks and then continue with estimation and reconstruction of the self-interference signal. Note that, for the low complexity of

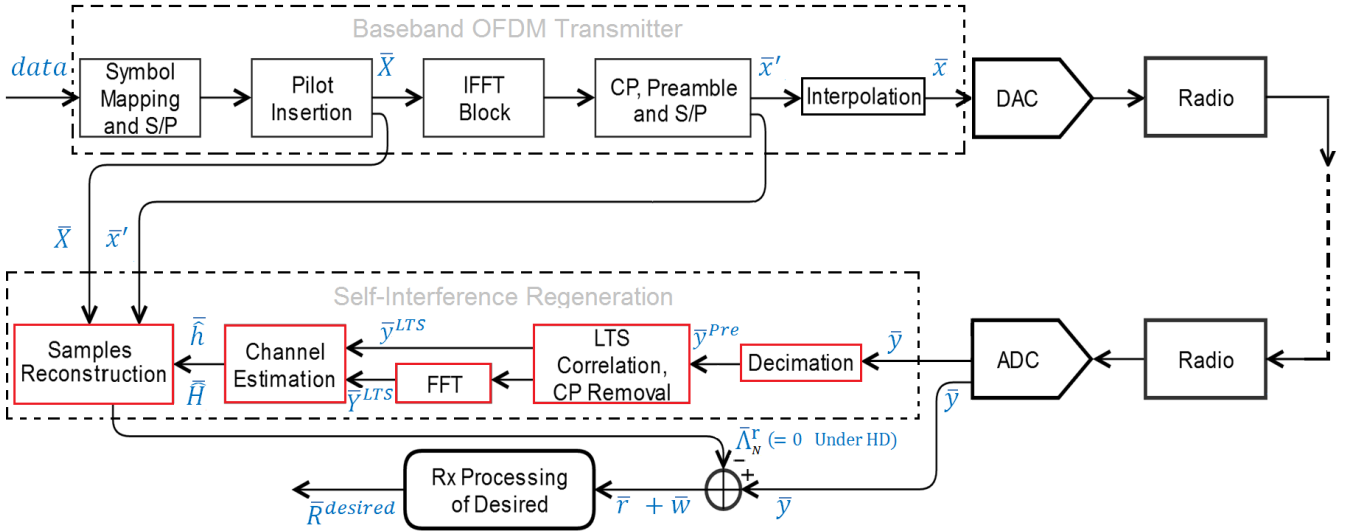


Fig. 5: System model of an 802.11a/g standard based full-duplex node.

full-duplex design, we are only considering linear digital cancellation to capture the channel effects, as described next.

A. System Model

Fig. 5 shows the structure of our full-duplex transceiver, which is based on IEEE 802.11a/g standard half-duplex OFDM system. To keep the system model general the RF interface in the figure is kept open ended. A list of key parameters of IEEE 802.11a/g standard that are included in our baseband model is presented in Table I. The transmission block of our full-duplex model is similar to a conventional half-duplex OFDM model, except for the known data symbols/samples (\bar{X}/\bar{x}') feed line in baseband for self-interference regeneration in digital domain on the receiving side. The baseband structure of our receiving side has some additional blocks (showed with red boxes in Fig. 5), which are essential prior to the receiver's processing of the desired signal. These additional units are required for self-interference regeneration $\bar{\Lambda}^r$ (an estimate) and performing its subtraction from total received signal \bar{y} , so that clean processing of the desired signal can be done. The baseband digital samples, \bar{y} at the output of the ADC can be written as

$$\bar{y} = \bar{x} * \bar{h} + \bar{r} + \bar{w}. \quad (1)$$

Here, \bar{h} is the channel impulse response corrupting the known transmitted samples \bar{x} , \bar{r} represents the desired signal samples

and \bar{w} is AWGN noise per sample. In (1) the channel \bar{h} includes both the transceiver chains and the multi-path channel impairments. For self-interference channel estimation process \bar{r} is assumed to be zero, i.e. $\bar{r} = 0$. Thus reducing (1) to

$$\bar{y} = \bar{x} * \bar{h} + \bar{w}. \quad (2)$$

In Fig. 5, after decimation, LTS symbols are extracted from the preamble \bar{y}^{Pre} , through LTS correlation procedure. These LTS symbols are averaged first, and then used to estimate the self-interference channel \bar{h} either in time or frequency domain, as shown in Fig. 5. In any case, the final reconstructed signal $\bar{\Lambda}^r$ is a time domain signal. The reconstructed self-interference samples are obtained as

$$\bar{\Lambda}^r = \bar{h} * \bar{x} \text{ or } \text{IFFT}_K \{ \bar{X} \cdot \bar{H} \}$$

where K represents the IFFT size. After performing the subtraction, the system is left with

$$\bar{y} - \bar{\Lambda}^r = \bar{r} + \bar{w} + \bar{x}^{re}$$

where \bar{x}^{re} is the residual self-interference, and basically marks the noise floor levels for the receiver's processing of the desired signal \bar{r} .

After the digital self-interference cancellation, the Rx processing (shown as a single block here) of the desired signal is performed in the standard fashion, i.e. first, coarse estimation of carrier frequency offset and timing recovery is done using short training sequence (STS) symbols, following that fine symbol synchronization and channel estimation is realized using LTS symbols embedded in the preamble of the desired signal. Afterwards, FFT processing and the equalization is performed, where the pilots are further used to compensate the residual frequency offset caused by phase rotation. In the final phase, the equalized data is de-mapped, de-interleaved, and decoded to obtain the desired symbols $\bar{R}^{desired}$.

As mentioned earlier, this work considers an OFDM based air interface, similar to the standard IEEE 802.11a/g, which has a preamble length of 12 symbols with the first 10 belong

TABLE I: Key Parameters of the IEEE 802.11a/g Standard used in our full-duplex design.

Modulation	BPSK, QPSK, 16-QAM
No of Subcarriers	52
No of Pilots	4
OFDM Symbol duration	4 μ s
Guard Interval	800 ns
Signal Bandwidth	16.66 MHz
Subcarrier Spacing	312.5 kHz
FFT Size	64

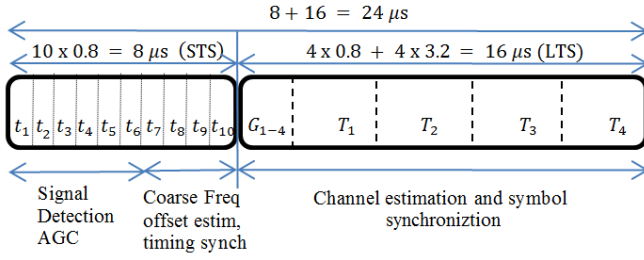


Fig. 6: Modified preamble structure of IEEE 802.11a/g standard with four LTS symbols.

to the STS symbol, and the remaining two belong LTS symbol. We further consider a modified preamble structure, where the number of LTS symbols are kept variable (e.g. 2, 4 symbols etc.) in order to investigate its effect on self-interference cancellation. Fig. 6 shows an example of modified preamble structure, with four LTS symbols.

B. Estimation of Self-Interference Channel

Channel estimation is the process of estimating the wireless channel taps \bar{h} that essentially distorts the transmitted signal before it actually reaches the receiver. To effectively complete this task in wireless systems, training sequence (transmitted on each sub-carrier) and/or pilots (transmitted on subset of carriers) are used, as they are fixed, known and typically carry the same channel effects as the actual data symbols. Different structures for the pilots and the training sequence symbols have been proposed and realized for real time implementation. In our full-duplex design a preamble structure similar to IEEE 802.11a/g is used, with the modification of varying number of LTS symbols, as shown in example Fig. 6.

1) *Least Square Frequency Domain Estimation:* The least square frequency domain estimation (LS-FDE) process in a wireless system is usually performed with LTS symbols transmitted on each sub-carrier, attached at the beginning of the payload. The estimation process starts by averaging of the received LTS samples, and since FFT is a linear operation, therefore averaging is done before the FFT operation i.e. in time domain. Henceforth, only one FFT operation is required to calculate the channel estimate. After the FFT processing, the received LTS symbols can be written as

$$\bar{Y}_L^{LTS} = \bar{X}^{LTS} \cdot \bar{H} + \bar{W}_L^{LTS}. \quad (3)$$

Here, L represents the number of LTS symbols, \bar{Y}_L^{LTS} is the average of L received LTS symbols, \bar{H} is the frequency response of the channel impulse response represented as \bar{h} in (2), \bar{X}^{LTS} is a vector containing transmitted LTS for each subcarrier and \bar{W}_L^{LTS} is the additive noise per sample. Our aim here is to find a least square based estimate of \bar{H} , and for that we need to minimize the argument, i.e.

$$\text{minimize} \|\bar{Y}_L^{LTS} - \bar{X}^{LTS} \cdot \bar{H}\|_2^2 = \text{MSE}. \quad (4)$$

Thus, the channel vector estimate $\bar{\hat{H}}$ is computed as given in [18];

$$\bar{\hat{H}} = \langle \bar{Y}_L^{LTS} \cdot / \bar{X}^{LTS} \rangle, \quad (5)$$

$$\bar{\hat{H}} = \bar{H} + \langle \bar{W}_L^{LTS} \cdot / \bar{X}^{LTS} \rangle. \quad (6)$$

Here (6) shows that the estimated channel is the sum of actual channel response \bar{H} and the imprecision in the estimate caused by the AWGN noise. The time domain channel impulse response can then be evaluated as

$$\bar{\hat{h}}^{\text{LS-F}} = \text{IFFT}_K \left\{ \bar{\hat{H}} \right\} \quad (7)$$

The LS-FDE scheme as given by (5) and (7) is used in [8], [11], [12] for digital cancellation.

2) *Least Square Time Domain Estimation:* The Least square time domain estimation (LS-TDE) approach obtains the channel estimate before FFT processing of the received LTS samples. This technique has been used in [5], [6] for the estimation of self-interference channel. In this estimation scheme, the channel impulse response \bar{h} is acquired. Based on (2), the average of L received LTS symbols \bar{y}_L^{LTS} is obtained as

$$\bar{y}_L^{LTS} = \bar{x}^{LTS} * \bar{h} + \bar{w}_L^{LTS} \quad (8)$$

For a fixed and predefined preamble, the time domain convolution in (8) can be expressed as a matrix multiplication, i.e.

$$\bar{y}_L^{LTS} = \mathbf{X}^{LTS} \bar{h} + \bar{w}_L^{LTS}, \quad (9)$$

In (9), \bar{h} is the channel impulse response vector and \mathbf{X}^{LTS} is the Toeplitz matrix formed using the known transmitted LTS samples as follows

$$\mathbf{X}^{LTS} = \begin{bmatrix} x_1 & x_n & x_{n-1} & \cdots & x_{n-P+2} \\ x_2 & x_1 & x_n & \cdots & x_{n-P+3} \\ \vdots & \vdots & \vdots & \ddots & \vdots \\ x_{n-1} & x_{n-2} & x_{n-3} & \cdots & x_{n-P} \\ x_n & x_{n-1} & x_{n-2} & \cdots & x_{n-P+1} \end{bmatrix} \bar{h} = \begin{bmatrix} h_1 \\ h_2 \\ \vdots \\ h_{P-1} \\ h_P \end{bmatrix}$$

In above expression, \mathbf{X}^{LTS} is a circular matrix of order $n \times P$, where the parameter P defines the maximum length of the channel impulse response and n represent the number of samples per OFDM symbol (same as FFT size K). Notice that the matrix \mathbf{X}^{LTS} can be pre-computed and stored because the LTS samples are fixed and known in advance. In our system, the length of the channel P is defined by the length of CP, which is specified as 800 ns, i.e. 16 samples, in Table I. In LS-TDE the goal is again to minimize the estimation error as in LS-FDE, but now, the processing is done in time domain. The channel impulse response estimate and mean square estimate (MSE) is thus calculated as shown in [18]

$$\bar{\hat{h}} = \mathbf{X}^{LTS \dagger} \bar{y}_L^{LTS} \quad (10)$$

$$\text{MSE} = \|\bar{\hat{h}} - \bar{h}\|_2^2 = \|\mathbf{X}^{LTS \dagger} \bar{w}_L\|_2^2.$$

Here $\mathbf{X}^{LTS \dagger}$ denotes Moore-Penrose (pseudo) inverse of \mathbf{X}^{LTS} and \bar{y}_L^{LTS} is the average of L LTS symbols. The channel frequency response estimate can then be obtained by performing FFT of the acquired impulse response as

$$\bar{\hat{H}}^{\text{LS-T}} = \text{FFT}_K \left\{ \bar{\hat{h}} \right\} \quad (11)$$

where the superscript in $\bar{\hat{H}}^{\text{LS-T}}$ represents that the estimate is obtained by taking K point FFT of the obtained estimate.

3) *FFT based Frequency Domain Estimation*: FFT based (FFT-FDE) channel estimation uses the LS-FDE as a starting point and it is essentially based on the fact that the energy in the time domain channel impulse response is usually concentrated in limited path (taps) [19]. Therefore, the estimate acquired with LS-FDE is first transformed into time domain through IFFT process to obtain time domain channel impulse response, i.e.

$$\tilde{h} = \text{IFFT}_K \{ \tilde{H} \}, \quad (12)$$

where \tilde{H} is the channel estimate obtained using (5) and \tilde{h} is channel impulse response obtained by taking K point IFFT. In (12), only the taps (paths) with significant energy are kept while the remaining forced to zero, as only noise exist in those taps. Thus, channel impulse response can be written as

$$\tilde{h}' = \begin{cases} \tilde{h} & 0 \leq n \leq P' \\ 0 & \text{otherwise} \end{cases} \quad (13)$$

In (13), \tilde{h}' is the modified channel impulse response and P' represent the significant energy taps. In our design P' is kept equal to CP with 16 samples that correspond to the duration of guard interval presented in Table I, i.e. $P' = P = 16$. This approach for obtaining time domain channel impulse response estimate is used in [8] for estimating the self-interference channel. The frequency domain channel estimate \tilde{H}^{FFT} can then be acquired by taking the K point FFT of \tilde{h}' as follows

$$\tilde{H}^{\text{FFT}} = \text{FFT}_K \{ \tilde{h}' \} \quad (14)$$

4) *Least Minimum Mean Square Error Frequency Domain Estimation (LMMSE-FDE)*: The LMMSE estimator uses the second-order statistics of the channel conditions i.e. channel correlation matrix and the least square estimate to further minimize the MSE. The LMMSE estimate can be presented as

$$\tilde{H}^{\text{LMMSE}} = \mathbf{W}_{X^{\text{LTS}}} \tilde{H},$$

$$\mathbf{W}_{X^{\text{LTS}}} = \mathbf{R}_{HH} (\mathbf{R}_{HH} + \sigma^2 (\tilde{X}^{\text{LTS}} \tilde{X}^{\text{LTS}H})^{-1})^{-1}, \quad (15)$$

where \mathbf{W}_X is the smoothing matrix that uses correlation properties of the channel to further improve \tilde{H} (the LS-FDE obtained through (5)). In (15) \mathbf{R}_{HH} is the auto-covariance matrix of the channel vector \tilde{H} , σ^2 is the AWGN noise variance, \tilde{X}^{LTS} are the known transmitted training symbols and the superscript $(\cdot)^H$ indicates Hermitian transpose. The LMMSE estimate is thus computed as given in [20]:

$$\tilde{H}^{\text{LMMSE}} = \mathbf{R}_{HH} (\mathbf{R}_{HH} + \sigma^2 (\tilde{X}^{\text{LTS}} \tilde{X}^{\text{LTS}H})^{-1})^{-1} \tilde{H}. \quad (16)$$

To obtain the estimate using (16) the knowledge of \mathbf{R}_{HH} (channel covariance matrix) and σ_n^2 (noise variance) is a major requirement, which makes LMMSE applications very limited in real-time communication systems as both of these parameters are mostly unknown, and in theory they are mostly assumed to be known.

C. Reconstruction of Self-Interference Signal

Reconstruction of the self-interfering signal is similar to the equalization procedure of wireless channels. In order to apply the channel effects on the reconstructed signal, the obtained channel estimate is processed with the known transmit data, so that the reconstructed signal innate the same channel impairments as that carried by the received self-interference signal.

1) *Frequency Domain Reconstruction*: The frequency domain reconstruction (FD-R) approach, which we have initially proposed in [14], processes the baseband symbols \tilde{X} (after pilot insertion, as shown in Fig. 5) with the frequency domain channel estimate \tilde{H} acquired using (5), (11), (14) or (16). The reconstructed frequency domain signal is obtained as

$$\tilde{\lambda}'_N = \tilde{H}_N \cdot \tilde{X}_N \rightarrow \tilde{\Lambda}'_N = \text{IFFT}_K \{ \tilde{\lambda}'_N \} \quad (17)$$

In (17) N defines the number of transmitted OFDM symbols, K represents the FFT size and $\tilde{\lambda}'_N$ gives the reconstructed N OFDM symbols in frequency domain. In order to equalize each transmitted OFDM symbol, the obtained channel estimate \tilde{H} , needs to be repeated N times. Once the symbols are equalized, they are transformed into time domain using IFFT, and then CP insertion, parallel to serial conversion, preamble attachment and interpolation is performed. Thus, the time domain self-interference samples $\tilde{\Lambda}'_N$ are reconstructed as illustrated in Fig. 7a.

2) *Time Domain Reconstruction*: Time domain reconstruction (TD-R) is the approach used in the existing full-duplex radio designs, presented in [5], [6], [12]. In this approach, the time domain transmitted samples \tilde{x}' (prior to interpolation filter as shown in Fig. 5) are convolved with the channel impulse response estimate \tilde{h} obtained using (10) or (13), so the resultant signal is given as

$$\tilde{\Lambda}'_N = \tilde{h} * \tilde{x}'. \quad (18)$$

Following the convolution operation the output $\tilde{\Lambda}'_N$ is interpolated to obtain the reconstructed signal $\tilde{\Lambda}'_N$ as presented in Fig. 7b.

Fig. 8, shows an example plot of self-interference reconstruction and suppression to the noise floor level, using

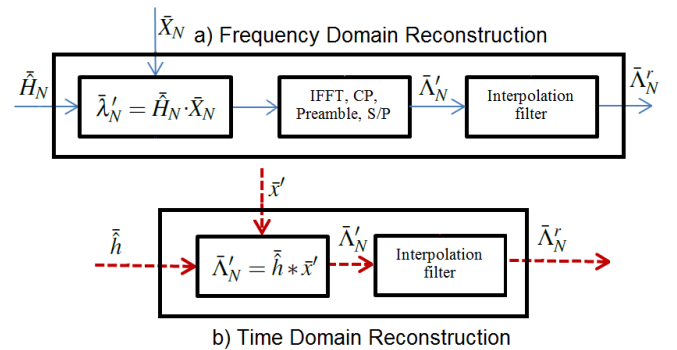


Fig. 7: Structure presenting the two approach for the reconstruction of self-interference signal in digital domain: a) Frequency domain reconstruction, b) Time domain reconstruction.

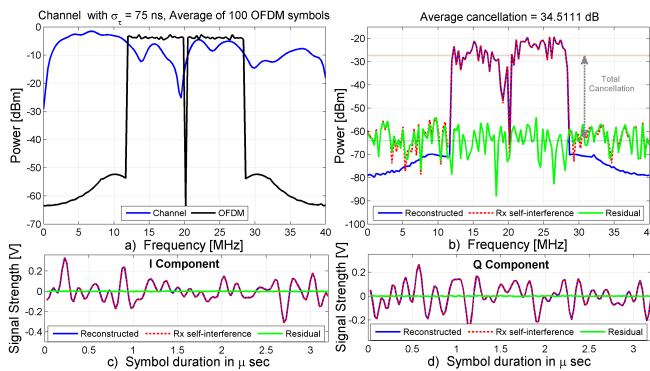


Fig. 8: Plot showing the self-interference reconstruction and suppression to the noise floor level. Plot (a) shows the transmitted OFDM symbol and the simulated highly selective fading channel in frequency domain. Likewise, Plot (b) presents the received OFDM symbol (in red), the reconstructed OFDM symbol (in blue) and the residual signal (in green). In plot (c) and (d), time domain I and Q components are presented respectively, with received OFDM symbol (in red), the reconstructed OFDM symbol (in blue) and the remaining signal (in green).

the proposed frequency domain reconstruction approach. Table II presents the summary of all digital self-interference cancellation techniques, including all the existing channel estimation techniques followed with the proposed frequency domain reconstruction and existing time domain reconstruction approaches. Here, the subscript in the representation indicates the type of reconstruction approach, i.e. 'T' denotes time domain reconstruction, and 'F' denotes frequency domain reconstruction, applied after the mentioned estimation techniques.

D. Performance Simulations

Fig. 9 presents the baseband model of the OFDM system shown in Fig. 5. This baseband model has specifically been used to evaluate and compare the performance of our proposed frequency domain reconstruction approach in terms of achieved digital self-interference cancellation, while employ-

TABLE II: Summary of digital self-interference cancellation techniques for full-duplex implementation.

Estimation	Frequency Domain Reconstruction	Time Domain Reconstruction
LS-TDE	LS-TDE _F proposed and its performance is evaluated in this work.	LS-TDE _T is used in [5], [6], its performance is evaluated for comparison in this work.
LS-FDE	LS-FDE _F proposed and its performance is evaluated in this work.	LS-FDE _T is used in [12], its performance is evaluated for comparison in this work.
FFT-FDE	FFT-FDE _F proposed and its performance is evaluated in this work.	Performed poorly even in AWGN channel, so it is not included in comparative performance evaluation.
LMMSE-FDE	LMMSE-FDE _F proposed and its performance is evaluated in this work.	Performed poorly even in AWGN channel, so it is not included in comparative performance evaluation.

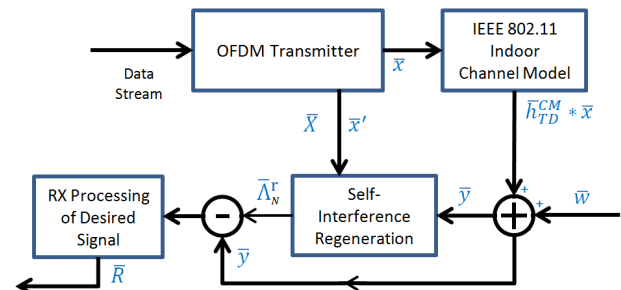


Fig. 9: Baseband system model used in the simulations.

ing different estimation techniques. In addition to the AWGN model, we have simulated a time dispersive slowly fading indoor channel model, which impinges the indoor fading environment on the OFDM packet.

1) *Channel Model*: The complex baseband representation of a time dispersive (multi-path) slowly fading, i.e., stationary or quasi stationary) channel impulse response is characterized by

$$h = \sum_{p=0}^{P_{\max}-1} \alpha_p \delta(t - T_p), \quad (19)$$

where α_p is zero-mean complex Gaussian random variable, T_p are the time delays of different multi-path and P_{\max} is the number of multi-path components. To apply the effects of multi-path fading channel on the transmitted OFDM signal in our system, we have employed IEEE 802.11 indoor channel model proposed in [21] that basically uses the exponential model for generating the power delay profile (PDP). In this model, the channel power decreases exponentially with delayed taps as follows:

$$A(p) = \frac{1}{\sigma_\tau} \exp^{-pT_s/\sigma_\tau}, \quad p = 0, 1, 2, \dots, P_{\max} \quad (20)$$

where σ_τ is the root mean square (RMS) delay spread, p is the discrete path index (taps) with P_{\max} as the index of the last path (with smallest non-negligible power) and T_s is the sampling time. In contrast to the exponential model in which the maximum excess delay is calculated by a path of the least non-negligible power level, the maximum excess delay in [21] is fixed as 10 times the RMS delay spread. In other words, the maximum number of paths is determined by σ_τ and T_s as

$$P_{\max} = \lceil 10\sigma_\tau/T_s \rceil.$$

Now, with the assumption that the power of the p^{th} channel tap has a zero mean and a variance of $\sigma_p^2/2$, the channel impulse response coefficients in (19) are obtained as:

$$\bar{h}_p = \bar{\gamma}_p + j\bar{\beta}_p, \quad p = 0, 1, 2, \dots, P_{\max} \quad (21)$$

In (21) $\bar{\gamma}_p$ and $\bar{\beta}_p$ are independent and identical Gaussian random variables, characterizing a multipath channel with components up to P_{\max} . Fig. 10 depicts a random realization of this channel model, with an RMS delay spread of 100 ns.

2) *Simulation Results*: For simulations, the OFDM system parameters are set according to Table I. One transmitted OFDM packet is carries 100 OFDM symbols with 16-QAM

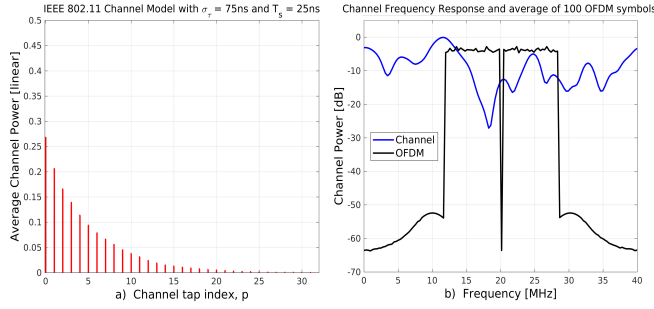


Fig. 10: A typical IEEE 802.11 indoor channel model realization for $\sigma_\tau = 75$ ns: (a) Channel power delay profile, (b) Channel frequency response.

modulation. To investigate the effect of the number of LTS symbols on the performance of digital self-interference cancellation, the variable LTS field in the modified preamble structure is increased from two to eight symbols. The channel model is simulated for 1000 random realizations, with PDP considered for different RMS delays spreads. The simulated channel conditions are then applied on the transmitted OFDM packet, and the digital self-interference cancellation performance is observed. The legend in each figure indicates the estimation techniques, with subscripts presenting the reconstruction approach and the numeric enclosed within the bracket representing the number of LTS symbols used.

First, the cancellation performance of all the discussed channel estimation schemes against the SNR of the received self-interfering signal in AWGN and flat fading channels, is observed. Fig. 11 depicts the amount of average digital cancellation achieved in pure AWGN channels, i.e. $h = 1$, zero dB channel power; Whereas, Fig. 12 presents digital cancellation performance under flat fading conditions with $\sigma_\tau = 10$ ns, and a coherence bandwidth B_c of ~ 20 MHz. It can be seen that from AWGN to flat fading channel there is a drastic degradation in the cancellation performance of LMMSE-FDE technique, certainly because of the smoothing matrix, which instead of improving the estimate acquired using LS-FDE, further distorted it. Likewise, the FFT-FDE technique is consistent with its poor cancellation performance regardless of the type of channel. Due to such poor performance even in AWGN and flat fading channels, after this point, the LMMSE-FDE and FFT-FDE techniques are not considered and discussed. Meanwhile, LS-TDE and LS-FDE techniques demonstrate superior digital self-interference cancellation up to the noise floor level, in both types of channels. Furthermore, with longer preamble, containing four LTS symbols a 0.5 – 1 dB more digital cancellation is observed. However, there is no considerable improvement in digital cancellation with lengths over four LTS symbols besides an undesirable contribution towards the overhead, so the plots with these lengths are not included in the subsequent results.

Secondly, frequency domain reconstruction and time domain reconstruction approach following LS-TDE and LS-FDE techniques are evaluated, under indoor fading channel considering different delay spreads. Fig 13 (a) and 13 (b), illustrate the digital self-interference cancellation in frequency

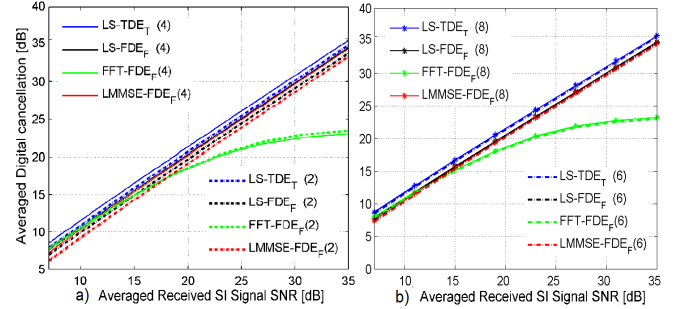


Fig. 11: Digital self-interference cancellation performance of the discussed estimation techniques in AWGN channel: (a) 2 and 4 LTS symbols, (b) 6 and 8 LTS symbols.

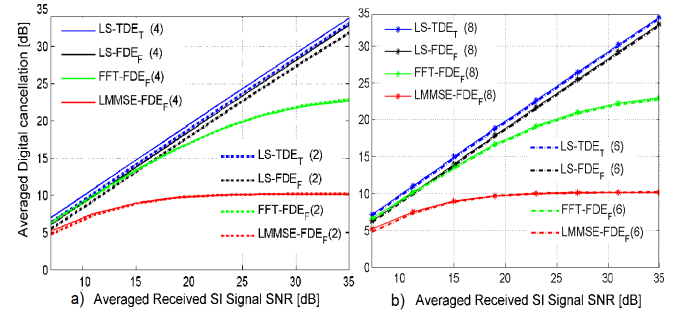


Fig. 12: Digital self-interference cancellation performance of the discussed estimation techniques under a flat channel with $\sigma_\tau = 10$ ns: (a) 2 and 4 LTS symbols, (b) 6 and 8 LTS symbols.

selective channels with coherence bandwidth of roughly 8 MHz and 2 MHz (considering a correlation of 0.5 and above), respectively. The results show that a larger delay spread degrades the performance of all the employed self-interference cancellation methods. Also, it can be noticed that the amount of digital cancellation increases with increasing SNR of the received self-interfering signal, which is logical because with a higher SNR, a better estimate can be obtained. This further indicates the performance limitation of digital cancellation for self-interfering signals with low SNR. Additionally, it can be seen that the time domain reconstruction approach with LS-FDE technique performs much poorer as compared to the

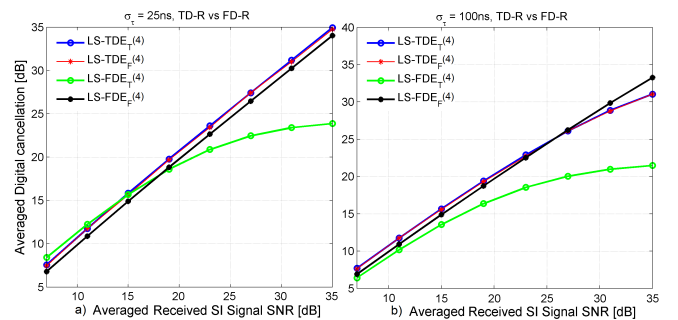


Fig. 13: Performance of digital self-interference cancellation techniques under frequency selective fading channels: (a) for $\sigma_\tau = 25$ ns, (b) $\sigma_\tau = 100$ ns.

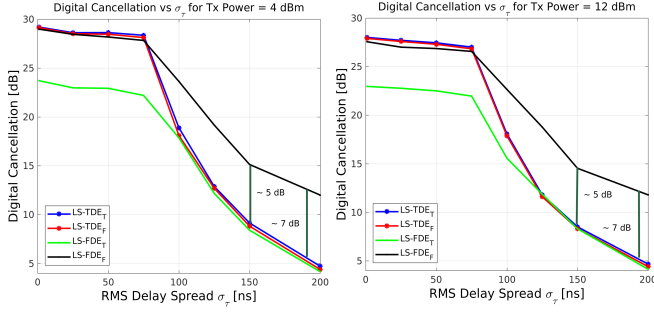


Fig. 14: Performance of digital self-interference cancellation techniques under time dispersive channel effects: (a) 36 dB received SNR, (b) 26 dB received SNR.

rest of the digital self-interference suppression approaches. The main reason for this degraded performance is that LS-FDE performs per carrier estimation, and taking the IFFT of the estimate distributes the concentrated power of channel taps to all K points of the IFFT, which distorts the channel impulse response estimate. This leads to poor reconstruction of the self-interfering signal, which consequently reduces digital cancellation.

Lastly, the digital cancellation performance of frequency domain reconstruction and time domain reconstruction approaches are analyzed against increasing RMS delay spread. The plots shown in Fig. 14 (a) and Fig. 14 (b) present the digital cancellation performance with LS-TDE and LS-FDE techniques, in channels with fixed SNR of 36 dB and 26 dB, respectively. In these results, the average achieved cancellation for both SNR levels is getting worse with increasing delay spread, which we have also seen in previous settings as well. Additionally, it can be observed that for large RMS delay spread, the digital cancellation observed with LS-TDE_T and LS-TDE_F, suffers far more than LS-FDE_F. This is due to the fact that for delay spreads larger than the duration of guard interval, LS-TDE technique fails to capture the channel impulse response efficiently, which eventually reduces the amount of digital cancellation; whereas LS-FDE technique, performs per carrier estimation, which makes it more resilient towards the selective nature of the channel.

E. Computational Complexity

In this section, we compare the digital cancellation algorithms in terms of computational complexity, which is measured as the number of floating point operations (flops) required to compute an instance of an algorithm. The computational requirement of the self-interference cancellation comprises of estimation complexity and reconstruction complexity, each of which can be further characterized as time and frequency domains approaches.

In [14], the computational requirements of the considered estimation and reconstruction algorithms based on (5), (10), (17) and (18) are derived. The summary of the obtained complexity expressions for digital self-interference cancellation algorithms are provided in the Table III. In the table, K represents the FFT/IFFT size, P is the estimated self-

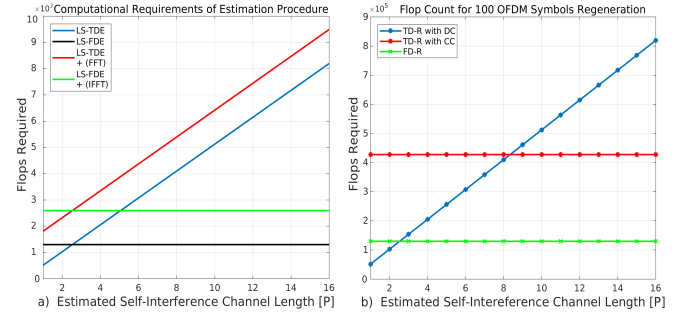


Fig. 15: Flop requirements of the self-interference regeneration process: (a) Estimation stage, (b) Reconstruction stage.

TABLE III: Computational Complexity of self-interference cancellation, considering the evaluated estimation and reconstruction methods.

Stage	Tech.	Computational Complexity Expressions	
		Real Multiplications	Real Additions
Est.	Time	$4(K \cdot P)$	$4(K \cdot P)$
	Freq.	$2K \log_2(K) - 7K + 12$	$3K \log_2(K) - 3K + 4$
Rec.	Time	$(4(K + CP) \cdot P) \cdot N$ (DC)	$(4(K + CP) \cdot P) \cdot N$ (DC)
		$(6K \log_2(K) - 17K + 36) \cdot N$ (CC)	$(9K \log_2(K) - 7K + 12) \cdot N$ (CC)
	Freq.	$(2K \log_2(K) - 3K + 12) \cdot N$	$(3K \log_2(K) - K + 4) \cdot N$

interference channel length, CP is for cyclic prefix, N denotes the number of OFDM symbols to be reconstructed, CC is short for the circular convolution, whereas DC is for direct convolution (two different convolution algorithms discussed in [14]). Fig. 15 presents the flop count for both estimation and reconstruction stages. As indicated by both figures, frequency domain based approaches are independent of the number of channel taps, while the complexity increases linearly when time domain estimation is employed.

Table IV presents a summary including the computational complexities and digital cancellation performances of the evaluated self-interference signal regeneration methods for 100 OFDM symbols each with 36 dB received SNR. In the table, the flop count is calculated for IEEE 802.11g standard, with an FFT size $K = 64$ and the channel length $P = 16$, defined by CP in the standard. It can be seen that the most efficient time domain reconstruction approach of circular convolution is roughly three times more expensive than the frequency domain reconstruction approach ($\sim 61\%$ reduction in the number of flops). Additionally, the superiority of the proposed frequency

TABLE IV: Computational complexities vs digital cancellation performance summary.

		Digital Cancellation in [dB] at 36 dB received SNR				
Digital Cancellation Technique	Flop count (Est. + Rec.)	Delay Spread σ_τ [ns]	25	75	100	200
LS-TDE _T	435392, (CC) $\rightarrow \sim 2.6x$		35.1	34.6	31.3	17.6
LS-TDE _F	176464 $\rightarrow \sim 1x$		35	34.4	31	17.6
LS-FDE _T	429792, (CC) $\rightarrow \sim 2.5x$		23.9	22.7	22.1	14
LS-FDE _F	169296 $\rightarrow 1x$		34.2	34	33.4	25

TABLE V: Computational Complexity of nonlinear self-interference cancellation.

Stage	Computational Complexity Expressions	
	Flops required for m^{th} order transformation of the transmitted samples	Flop count (real additions + multiplications) for time ¹ and frequency ² domains
Est.	$\sum_m (m-1).6K$	$[8(K.P).(m+1)/2]^1$ $[(5K\log_2(K)-12K+16).(m+1)/2]^2$
Rec.	$\sum_m (m-1).(K+CP).6N$	$[N.(15K\log_2(K)-24K+48).(m+1)/2]^1$ for circular convolution (CC) $[N.(5K\log_2(K)-4K+16).(m+1)/2]^2$

domain reconstruction approach in terms of digital cancellation performance (5 – 7 dB more digital cancellation) under extreme fading conditions, makes it more suitable for outdoor implementation, where large delay spreads are expected. These results clearly asserts frequency domain reconstruction as a more efficient and much simpler approach over time domain reconstruction approach.

At this point, we would also like to elaborate on how much the complexity of digital cancellation is increased when nonlinear cancellation is included. For this purpose we consider the nonlinear cancellation algorithm in [3], [6], where the residual self-interference is modeled as the weighted sum of nonlinearly transformed transmitted LTS samples. From the Fourier analysis of the received self-interference signal, it is observed that only odd components (x, x^3, x^5, \dots) are the ones with non-zero energy, hence the residual self-interference is modeled as

$$\bar{y}_{LTS} = \bar{x}_{LTS}(|\bar{x}_{LTS}|)^{m-1} * \bar{h}_m, \quad m \in \text{odd terms} \quad (22)$$

where \bar{x}_{LTS} are the transmitted LTS samples, \bar{h}_m are the distortion coefficients for some m^{th} order and \bar{y}_{LTS} are received LTS samples. The self-interference signal is then reconstructed as

$$\bar{\Lambda}'_N = \sum_{m \in \text{odd terms}} \bar{h}_m * \bar{x}'(|\bar{x}'|)^{m-1}. \quad (23)$$

In above equation, $\bar{\Lambda}'_N$ are the N reconstructed OFDM symbols, carrying the distortion effects of up-to m^{th} nonlinear order¹, \bar{h}_m are the estimated distortion coefficients and \bar{x}' are the transmitted samples (before 2x interpolation). From a simple analysis of (22) and (23), it can be seen that to reconstruct a self-interference signal with up-to m nonlinear components, each and every transmitted sample \bar{x}'/\bar{x}_{LTS} is required to be translated to m^{th} order first, introducing additional runtime complex multiplications for each sample, which are not required in linear cancellation. Table V presents the computational complexity expressions for self-interference estimation and reconstruction. It can be noticed that, the case for $m = 1$ stands for linear self cancellation alone and nonlinear cancellation is not there, so no transformation of the transmitted samples is required, and the total flop count expressions are same as the linear digital cancellation expressions presented earlier in Table III. However, for any other higher order self-interference reconstruction, additional flops for the transformation of the transmitted samples are required, increasing the

¹In [6] 'm' is selected as $m = 11$. However, in this paper, to keep the discussion general, no upper limit is specified for m .

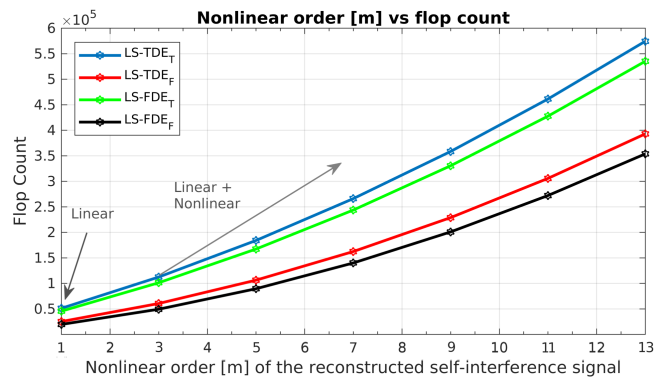


Fig. 16: Total flops required for transformation (of transmitted samples), estimation and reconstruction as a function of nonlinearity order m .

computational complexity as $O(2^{m-1} \cdot N)$. Fig. 16 depicts the flop count with increasing orders of nonlinear self-interference reconstruction on top of the evaluated linear cancellation algorithms, for $K = 64, P = 16, N = 10$ and $CP = 16$, where it can be observed that complexity of digital cancellation grows significantly with increasing m . Considering the odd orders, for the simplest case, $m = 3$, the number of flops is twice the number of flops required for linear cancellation alone. In this work, to keep our design simple, efficient and computationally less expensive, we have chosen not to implement the nonlinear self-interference cancellation.

IV. INTEGRATION OF SELF-INTERFERENCE SUPPRESSION STAGES FOR FULL-DUPLEX IMPLEMENTATION

For the implementation of our full-duplex design, we have considered a software defined radio i.e., WARP (v3) mango boards [22]. The WARP (v3) boards can support IEEE 802.11a/g standard for WiFi as their radio chains operate in 2.4 and 5 GHz wireless bands with 20 MHz bandwidth, and have a maximum of 25 dBm average transmit power with a noise floor of around -85 dBm. It enables rapid physical layer prototyping by utilizing the WARP hardware (baseband buffers and RF chains for carrying Tx/Rx samples),

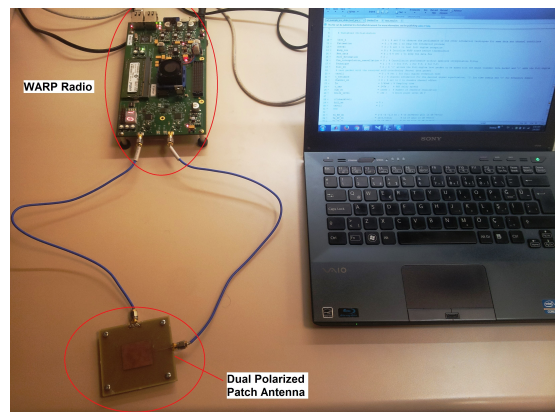


Fig. 17: Experimental setup of our full-duplex design.

and MATLAB signal processing. Fig. 17 shows the prototype of our full-duplex design, where self-interference is neutralized by integrating the two stages of self-interference suppression, presented in the earlier sections.

The first passive suppression stage involves the slot coupled antenna that can provide suppression of 56 – 60 dB, as discussed in Section II. The actual fabricated dual port, dual polarized slot coupled antenna is shown in Fig. 18. As can be seen in Fig. 18(b), the microstrip feed line is placed under the ground plane, and the ground plane with rectangular slot is sandwiched between two 1.6mm thick FR-4 dielectric layers.

As the second stage, digital domain cancellation algorithms discussed in Section III, are implemented on the WARP radio board via the WARPLAB 7 reference design [23]. WARPLAB 7 provides an interface between the MATLAB environment of the host PC and WARP board peripherals, including the radio transceiver chains. This way, in-phase and quadrature phase (IQ) samples generated in the MATLAB environment are delivered to the board peripherals via Ethernet and vice-versa. For enabling full-duplex communication, we have implemented the complete WiFi OFDM standard by realizing the modified OFDM system model presented in Fig. 5, and the discussed digital cancellation algorithms. Since the employed antenna prototype works only in 2.4 GHz band, the current implementation only supports both IEEE 802.11a and IEEE 802.11g standards in 20 MHz bandwidth; however, by adjusting the radio bandwidth and the antenna settings appropriately, our design can be easily extended to other WiFi standards as well.

V. TEST RESULTS

For evaluating the performance of our full-duplex design, we have performed detailed experiments with integrated setup of WARP radio and patch antenna. The parameters of our experimental setup can be classified into baseband OFDM transmission settings, RF settings and channel emulator settings. The baseband OFDM transmission settings are the same as in IEEE 802.11a/g standard as listed in Table I; however, the results presented here are only for 16-QAM and with four LTS symbols. Each transmission burst contains 700 OFDM symbols plus the preamble. Four digital self-interference cancellation techniques (LS-TDE_T, LS-FDE_T, LS-TDE_F and LS-FDE_F) discussed in Section III, are implemented for performance evaluation with WARP (v3) board.

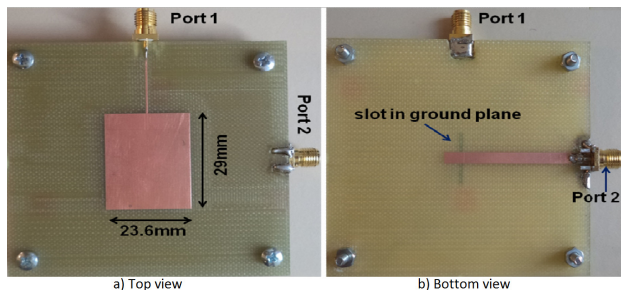


Fig. 18: Top and bottom view of the implemented slot coupled antenna.

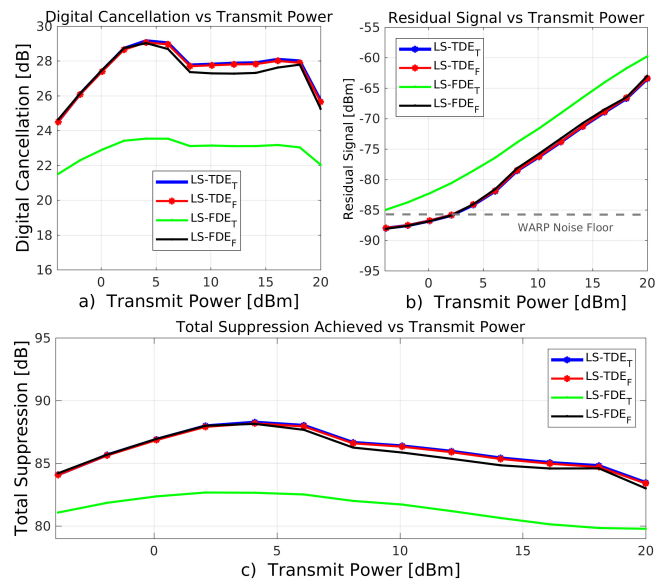


Fig. 19: Performance of the proposed full-duplex design for different digital cancellation techniques with WiFi 802.11g signal transmissions in the range of transmit power levels, which are varied from -4 dBm to 20 dBm.

The RF settings include the transmission band selection, which is channel 9 of IEEE 802.11g standard with 2.452 GHz center frequency (20 MHz bandwidth), and the total transmit power increased from -4 dBm to 20 dBm. For each transmit power level, we have done 100 transmissions, and then the average cancellation over all transmissions is computed.

Fig. 19 demonstrates the self-interference suppression performance of our proposed design for power levels between -4 dBm to 20 dBm. From the three plots in this figure, it can be seen that the performance of the proposed LS-FDE_F technique in the experimental setup is roughly similar to LS-TDE_T technique, and it outperforms the LS-FDE_T approach. These results are consistent with our simulation results presented earlier in Section III-D. Also, it can be observed that with increasing transmit power levels, the digital cancellation capability of all the employed techniques tend to decrease, instead of improving, and the reason for this degradation is the nonlinear behavior of the RF amplifiers at higher gains. Since only linear digital cancellation is employed in this design, the residual signal strength is increased at high transmit power levels, as depicted in Fig. 19(b), reducing the total suppression at these power levels as shown in Fig. 19(c). Note that, following the linearly increasing part of Fig. 19(c) curve, the system can reach the desired amount (105 dB) of total suppression to bring 20 dBm transmit power level to -85 dBm, i.e. the noise floor. By applying analog cancellation and nonlinear digital cancellation with this current design, suppression of self-interference to the noise floor can be achieved. However, analog cancellation requires extra circuitry and nonlinear digital cancellation requires computationally complex algorithm, both of which will significantly increase the implementation complexity and the size of this design.

Fig. 20 presents the digital cancellation performance plot

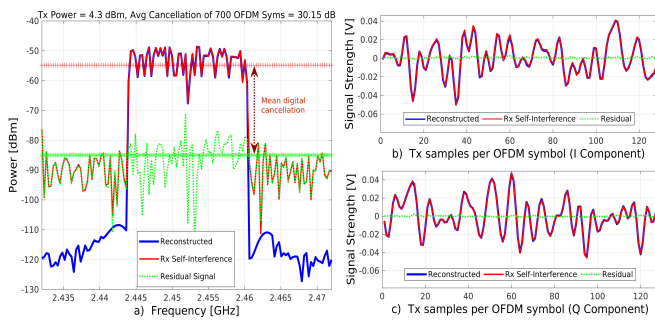


Fig. 20: Per symbol cancellation plot: (a) Frequency domain response, (b) Time domain I and Q waveforms.

with WARP radio. The single OFDM symbol spectrum (out of 700 symbols) in the figure, presents the received self-interference signal strength after passive suppression of ~ 58 dB in red. The spectrum in blue is the reconstructed OFDM symbol, and the spectrum in green is the residual self-interference signal with strength -84.6 dBm, after digital cancellation of 30 dB. In plot (b) and (c), time domain I and Q components are shown respectively, with received OFDM symbol (in red), the reconstructed OFDM symbol (in blue) and the residual signal (in green).

With the goal of implementation simplicity, the proposed design can introduce full-duplex to existing IEEE 802.11a/g equipment by only connecting the slot coupled antenna and implementing the proposed digital cancellation algorithm LS-FDE_F in baseband, with only fragments of changes in the digital hardware. Our full-duplex design has demonstrated self-interference suppression to the radio’s noise floor for transmit power levels up-to 4 dBm, suggesting its applications in low power wireless systems.

In order to further evaluate the performance of the our full-duplex design in a multi-path fading environment, we employed a channel emulator on the baseband samples received from the WARP radio’s receiving chain buffers. For this purpose, using the IEEE 802.11 indoor channel model discussed in Section III-D1, first multi-path fading channels for different RMS delay spread values (between 1 ns to 200 ns) are generated, and then these channel effects are imposed on the received IQ samples. The performance results are

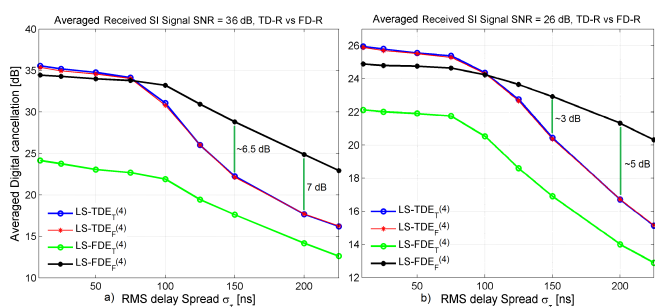


Fig. 21: Performance of the digital cancellation under multi-path fading channels, where the RMS delay spread is varied from frequency flat channels to frequency selective channels.

obtained for two different transmit power levels, i.e. 4 dBm and 12 dBm, and the averaged digital cancellation achieved from 1000 random channel realizations for each RMS delay spread is shown in Fig. 21(a) and Fig. 21(b). In the figure, 5 – 7 dB better cancellation performance of the proposed LS-FDE_F can be observed, especially for large RMS delay spreads, which agrees with results presented in the simulations section. These test results further verifies the advantage of our proposed digital cancellation technique in outdoor full-duplex implementation, where large delay spread levels are observed. These results are promising for a more complex full-duplex design involving nonlinear cancellation; however, for the sake of simplicity our current design does not incorporate nonlinear cancellation, and supports low power full-duplex communications.

VI. CONCLUSIONS

In this work, we have presented a simple full-duplex design, which, unlike the existing full-duplex radios in the literature, eliminates the requirement of additional and complex hardware for self-interference suppression and cancellation. Our design uses a single patch antenna without any duplexer or circulator element, providing 56 – 60 dB of passive suppression. For the mitigation of residual self-interference after the passive suppression stage, we propose to employ a frequency domain based estimation and reconstruction technique for self-interference regeneration in the digital domain, which has shown to offer a computational complexity reduction of 61% over the existing time domain techniques.

The proposed full-duplex design provides a total self-interference suppression of 88 dB, which is adequate for low power or short range full-duplex communication, and our digital cancellation technique is shown to be resilient to multi-path fading by demonstrating 5 – 7 dB higher digital cancellation in highly frequency selective channels. The proposed full-duplex implementation can easily facilitate full-duplex communication in IEEE 802.11 or any other OFDM based system, since it only requires minimal changes in the digital baseband hardware and just a single antenna. Provided that the nonlinear effects of the RF amplifier are taken into account in later designs, the total suppression can be improved further, which can increase communication range, where the shown advantages of multi-path resiliency can be realized.

REFERENCES

- [1] Z. Zhang, K. Long, A. V. Vasilakos, and L. Hanzo, “Full-duplex wireless communications: challenges, solutions, and future research directions,” *Proceedings of the IEEE*, vol. 104, no. 7, pp. 1369–1409, 2016.
- [2] A. Sabharwal, P. Schniter, D. Guo, D. W. Bliss, S. Rangarajan, and R. Wichman, “In-band full-duplex wireless: Challenges and opportunities,” *IEEE Journal on Selected Areas in Communications*, vol. 32, no. 9, pp. 1637–1652, 2014.
- [3] D. Korpi, J. Tamminen, M. Turunen, T. Huusari, Y.-S. Choi, L. Anttila, S. Talwar, and M. Valkama, “Full-duplex mobile device: pushing the limits,” *IEEE Communications Magazine*, vol. 54, no. 9, pp. 80–87, 2016.
- [4] H. Zhuang, J. Li, W. Geng, and X. Dai, “Duplexer design for full-duplex based wireless communications,” *China Communications*, vol. 13, no. 11, pp. 1–13, 2016.
- [5] D. Bharadia and S. Katti, “Full duplex mimo radios,” in *11th USENIX Symposium on Networked Systems Design and Implementation (NSDI 14)*, pp. 359–372, 2014.

- [6] D. Bharadia, E. McMillin, and S. Katti, "Full duplex radios," *ACM SIGCOMM Computer Communication Review*, vol. 43, no. 4, pp. 375–386, 2013.
- [7] J. Zhou, N. Reiskarimian, J. Diakonikolas, T. Dinc, T. Chen, G. Zussman, and H. Krishnaswamy, "Integrated full duplex radios," *IEEE Communications Magazine*, vol. 55, no. 4, pp. 142–151, 2017.
- [8] E. Ahmed, A. M. Eltawil, and A. Sabharwal, "Self-interference cancellation with nonlinear distortion suppression for full-duplex systems," in *2013 Asilomar Conference on Signals, Systems and Computers*, pp. 1199–1203, IEEE, 2013.
- [9] E. V. Rogozhnikov, A. S. Koldomov, and V. A. Vorobyov, "Full duplex wireless communication system, analog cancellation: Review of methods and experimental research," in *Control and Communications (SIBCON), 2016 International Siberian Conference on*, pp. 1–5, IEEE, 2016.
- [10] E. Everett, A. Sahai, and A. Sabharwal, "Passive self-interference suppression for full-duplex infrastructure nodes," *IEEE Transactions on Wireless Communications*, vol. 13, no. 2, pp. 680–694, 2014.
- [11] E. Ahmed and A. M. Eltawil, "All-digital self-interference cancellation technique for full-duplex systems," *IEEE Transactions on Wireless Communications*, vol. 14, no. 7, pp. 3519–3532, 2015.
- [12] M. Jain, J. I. Choi, T. Kim, D. Bharadia, S. Seth, K. Srinivasan, P. Levis, S. Katti, and P. Sinha, "Practical, real-time, full duplex wireless," in *Proceedings of the 17th annual international conference on Mobile computing and networking*, pp. 301–312, ACM, 2011.
- [13] M. Duarte, C. Dick, and A. Sabharwal, "Experiment-driven characterization of full-duplex wireless systems," *IEEE Transactions on Wireless Communications*, vol. 11, no. 12, pp. 4296–4307, 2012.
- [14] M. S. Amjad and O. Gurbuz, "Linear digital cancellation with reduced computational complexity for Full-Duplex radios," in *2017 IEEE Wireless Communications and Networking Conference (WCNC) (IEEE WCNC 2017)*, (San Francisco, USA), IEEE, Mar. 2017.
- [15] H. Nawaz and I. Tekin, "Three dual polarized 2.4 ghz microstrip patch antennas for active antenna and in-band full duplex applications," in *Microwave Symposium (MMS), 2016 16th Mediterranean*, pp. 1–4, IEEE, 2016.
- [16] D. M. Pozar, "Microstrip antenna aperture-coupled to a microstripline," *Electronics letters*, vol. 21, no. 2, pp. 49–50, 1985.
- [17] M. P. David, "A review of aperture coupled microstrip antennas: History, operation, development, and applications by," 1996.
- [18] J. Terry and J. Heiskala, *OFDM wireless LANs : a theoretical and practical guide*. Indianapolis, Ind. Sams, 2002. OFDM : Orthogonal Frequency Division Multiplexing.
- [19] Y. Kang, K. Kim, and H. Park, "Efficient dft-based channel estimation for ofdm systems on multipath channels," *IET communications*, vol. 1, no. 2, pp. 197–202, 2007.
- [20] O. Edfors, M. Sandell, J.-J. Van de Beek, S. K. Wilson, and P. O. Borjesson, "Ofdm channel estimation by singular value decomposition," *IEEE Transactions on communications*, vol. 46, no. 7, pp. 931–939, 1998.
- [21] N. Chayat, "Ieee 802.11-97/96," September, 2014.
- [22] "Warp project." <http://warpproject.org>, 2017. [Online; accessed 2-March-2017].
- [23] "Warplab 7 reference design, warp v3 sdr, mango board." <http://warpproject.org/trac/wiki/WARPLab>, 2017. [Online; accessed 2-March-2017].



Muhammad Sohaib Amjad received his MSc Electronic Engineering from Sabanci University, Istanbul, Turkey in 2016. He completed his BSc Electrical Engineering from Air University, Pakistan in 2011. From 2011 to 2014, he worked as a Lab Engineer in EE Dept. of Air University. Currently, he is working as a scientific researcher in CCS labs, University of Paderborn, Germany. His research interests include wireless communications, signal processing and full duplex wireless design.



Dr. Haq Nawaz has received his PhD in Electronic Engineering from Sabanci University, Istanbul, Turkey. He completed his BSc Electrical Engineering and Master in Telecommunication Engineering from University of Engineering and Technology (UET) Taxila, Pakistan in 2005 and 2012 respectively. From 2006 to 2009, he was with SUPARCO Pakistan as RF and Microwave Design Engineer. He served UET Taxila, Sub-campus Chakwal, Pakistan as Lecturer Electronics Engineering from 2010 to 2012. Currently, he is a Post-doc research fellow with Faculty of Engineering and Natural Sciences (FENS), Sabanci University, Istanbul, Turkey. His research interests include full duplex antenna design, RF circuits design and measurements for Radar and Satellite systems and indoor positioning/localization systems design.



Kerem Özsoy has received his B.S. degree in Microelectronics Engineering from Sabanci University in 2007 and his M.S. degree in Electronics Engineering from Sabanci University in 2009. After graduation he has worked in the electronic industry as a researcher and team leader. He is one of the co-founder of Antsis Elektronik. Since 2014 he is working as a design engineer in Antsis Elektronik. His research interests include antenna, RF, microwave and millimeter circuits design.



Dr. Özgür Gürbüz received her B.S. and M.S degrees in Electrical and Electronics Engineering at Middle East Technical University, in 1992 and 1995, respectively. She received her Ph.D. degree in Electrical and Computer Engineering from Georgia Institute of Technology in 2000. In her Ph.D. thesis, she worked on power control schemes for multimedia support in 3G W-CDMA wireless systems. From 2000 until 2002 she worked as a researcher for Cisco Systems, in Wireless Access and Wireless Networking Business Units. As of September 2002,

Dr. Gurbuz joined the Faculty of Engineering and Natural Sciences at Sabanci University, where she is currently serving as an Associate Professor. Her research interests remain in the field of wireless communications and networks, in particular, medium access control, scheduling, radio resource management and cross layer design for maximizing the network level performance of evolving wireless technologies. Lately, she has been working on in-band full duplex wireless communications and networking. She is a member of IEEE and IEEE Communications Society.



Dr. Ibrahim Tekin received his B.S and M.S degrees from Electrical and Electronics Engineering Department of Middle East Technical University (METU) in 1990 and 1992, respectively. From 1993 to 1997, he was with the Electrical Engineering Department of the Ohio State University (OSU) where he received his Ph.D degree in 1997. 1997 to 2000, he worked as a researcher in Wireless Technology Lab of Bell Laboratories, Lucent Technologies. He is now with the Electronics Engineering program at Sabanci University, Istanbul. His research interests are in RF and microwave circuit design, millimeter wave antennas and circuits. He is involved in various projects including Indoor positioning using GPS signals, 77 GHz LNA and antenna design, RFIC design for WLAN systems, antennas for full duplex systems. He is a senior member of IEEE Antennas and Propagation society.